Isotopic homogeneity of iron in the early solar nebula

X. K. Zhu, Y. Guo, R. K. O'Nions, E. D. Young & R. D. Ash

Department of Earth Sciences, University of Oxford, Parks Road, Oxford OX1 3PR, UK

The chemical and isotopic homogeneity of the early solar nebula, and the processes producing fractionation during its evolution, are central issues of cosmochemistry. Studies of the relative abundance variations of three or more isotopes of an element can in principle determine if the initial reservoir of material was a homogeneous mixture or if it contained several distinct sources of precursor material. For example, widespread anomalies[1–4] observed in the oxygen isotopes of meteorites have been interpreted as resulting from the mixing of a solid phase that was enriched in ^{16}O with a gas phase in which ^{16}O was depleted[1–3], or as an isotopic 'memory' of Galactic evolution[5]. In either case, these anomalies are regarded as strong evidence that the early solar nebula was not initially homogeneous. Here we present measurements of the relative abundances of three iron isotopes in meteoritic and terrestrial samples. We show that significant variations of iron isotopes exist in both terrestrial and extraterrestrial materials. But when plotted in a three-isotope diagram, all of the data for these Solar System materials fall on a single mass-fractionation line, showing that homogenization of iron isotopes occurred in the solar nebula before both planetesimal accretion and chondrule formation.

The significance of the oxygen-isotope anomalies observed in meteorites with regard to early Solar System history remains the subject of active debate. It has been demonstrated experimentally that the observed anomalies could be produced by chemical reactions within a homogeneous gaseous reservoir[6,7]. Indeed, it has been observed that mass-independent fractionation of oxygen isotopes is widespread in the Earth's atmosphere[7–9]. More recent studies have shown that such oxygen-isotope anomalies induced by chemical reactions between gas phases can be transferred to terrestrial solid phases[10,11]. Thus the existence of oxygen-isotope anomalies can no longer be regarded as evidence of the heterogeneity of the early solar nebula.

To constrain issues such as the chemical and isotopic homogeneity in the early solar nebula, investigation of the isotopic composition of elements other than oxygen is therefore needed. Thanks to recent advances in mass spectrometry, the opportunity now exists to investigate the patterns of isotopic variation in a range of other elements of different volatility. Among these elements, iron is a particularly interesting target. It is a major element in terrestrial planets, and has four naturally occurring stable isotopes, ^{54}Fe, ^{56}Fe, ^{57}Fe and ^{58}Fe. These isotopes are produced at the explosive silicon-burning stage of stellar evolution[12]. Isotopes of iron are produced in different proportions in different stars, and the average isotopic composition of the interstellar medium changes with time during Galactic evolution (D. D. Clayton, at http://photon.phys.clemson.edu/joel/claytonZ/). Variation patterns of iron isotopes resulting from nucleosynthetic processes are significantly different from those caused by mass-dependent fractionation (see above). Thus iron isotopes are expected to be useful tracers in constraining the degree of initial isotopic homogeneity of the solar nebula. Realization of this potential has been largely hampered by the absence of suitable techniques for precise isotope measurements. The introduction of plasma source mass spectrometry is rapidly advancing the techniques of isotope analysis[13–17], and a technique for high-precision measurement of the $^{57}Fe/^{54}Fe$ ratio has been developed recently[15,16]. Here the technique is developed further, and we present the results of measurements of the $^{56}Fe/^{54}Fe$ and $^{57}Fe/^{54}Fe$ ratios in terrestrial and extraterrestrial materials.

We have sampled a wide variety of meteorite types, representing different parent bodies. These include chondrites (carbonaceous, ordinary, and enstatite chondrites), achondrites (aubrite, eucrite, ureilite, and Shergotty–Nakhla–Chassigny (SNC) meteorite), pallasites, and iron meteorites. We performed measurements of iron isotopes on chondrules, matrices, metal fractions, or bulk samples. Chondrules were hand-picked from the meteorites after gentle crushing, and freed from matrix coating by air abrasion and ultrasonic cleaning. For reference purposes, we also analysed a selection of iron-containing minerals—haematite, magnetite and siderite. Silicate meteoritic materials were digested in concentrated HF and HNO_3, iron meteorites in 2 M HCl, and terrestrial minerals in 6 M HCl. All samples were purified by ion exchange separation following complete digestion[15]. Iron-isotope analyses were performed on a Nu Instruments plasma source mass spectrometer, using a standard–sample–standard procedure similar to that described previously[14–16]. The isobaric interferences of $[^{14}N^{40}Ar]^+$ and $[^{16}O^{40}Ar]^+$ with the ^{54}Fe and ^{56}Fe signals were reduced to a negligible levels. This was done by matching concentrations of Fe in standard and sample solutions to within 20%, and by desolvating samples using a CETAC MCN-6000 nebulizer without N_2 flow. Measured $^{56}Fe/^{54}Fe$ and $^{57}Fe/^{54}Fe$ ratios are expressed in terms of $\epsilon^{56}Fe$ and $\epsilon^{57}Fe$, which are deviations in parts per 10^4 from the Fe isotope reference material IRMM-14. Results are presented in Table 1.

These materials show overall variations of ~16 and ~23 ϵ-units in $^{56}Fe/^{54}Fe$ and $^{57}Fe/^{54}Fe$ ratios, respectively, with $\epsilon^{56}Fe$ ranging from −6.1 to 9.8, and $\epsilon^{57}Fe$ varying from −8.8 to 14.1 (Table 1). Within the meteoritic samples, the chondritic materials show relatively large variations with $\epsilon^{57}Fe$ ranging from −8.8 to 9.3, whereas achondrites and pallasites display much smaller variations with $-2.1 \leq \epsilon^{57}Fe \leq 2.0$, and iron meteorites are particularly homogeneous with $\epsilon^{57}Fe$ varying from 0.6 to 2.0 only. These results for iron meteorites are indistinguishable from the data reported previously for the same samples[16], where only $^{57}Fe/^{54}Fe$ ratios had been measured. The consistency between these two data sets shows the robustness of the analytical techniques used. The smaller variation of iron isotopes in achondrites, pallasites and iron meteorites compared to chondritic materials could be due to isotope re-equilibration having occurred within the parent bodies.

When plotted on a three-isotope diagram, all iron-isotope data

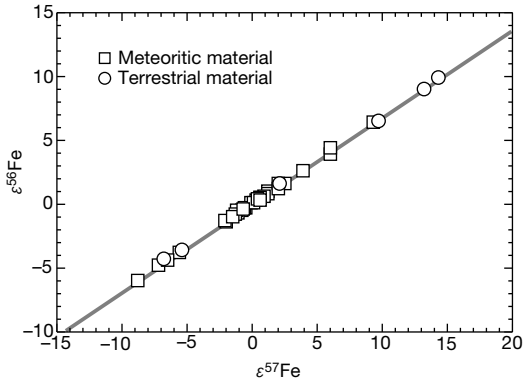

Figure 1 A three-isotope plot for iron, showing that all the Fe-isotope data from both terrestrial and extraterrestrial materials plot on a single mass-fractionation line. The correlation between $\epsilon^{56}Fe$ and $\epsilon^{57}Fe$ is $\epsilon^{56}Fe = (0.677 \pm 0.004)\epsilon^{57}Fe$, and $r^2 = 0.999$. If the regression is not forced through the origin, then $\epsilon^{56}Fe = (0.678 \pm 0.004)\epsilon^{57}Fe - 0.034$, with $r^2 = 0.999$. The size of data points represents the analytical uncertainty, which is defined as two standard deviations of long-term repeatability.

define a single line that passes through the origin with a slope of ~0.68 (Fig. 1). This observation is entirely consistent with theoretical expectations if the iron-isotope compositions in all analysed materials evolved from a single isotopically uniform reservoir in a mass-dependent manner. As the samples analysed are ultimately derived from different parent bodies, the iron-isotope homogenization cannot be attributed to processes occurring within the parent bodies themselves. Thus the observation of this single mass-fractionation line shows that all the iron in both terrestrial and extraterrestrial materials analysed were derived ultimately from a single isotopically homogeneous reservoir—which existed before the formation of chondrules and parent bodies.

Extraterrestrial samples analysed in this study cover all the main known meteorite types, and probably represent 14 different parent bodies including the Earth and Mars. Thus there is good reason to believe that the iron isotopes recorded in these samples are representative of Solar System materials. Furthermore, the measured samples include meteorites that are amongst the most anomalous materials from the oxygen isotope point of view, and they exhibit the full range in oxygen isotope ratios observed for bulk meteorites. For example, the meteorite with the most ^{16}O-rich bulk composition is the pallasite Eagle Station, with $\Delta^{17}O = -4.51‰$ (refs 18, 19); $\Delta^{17}O$ are deviations of $^{17}O/^{16}O$ ratios from the terrestrial mass fractionation line. The most depleted is LL3 chondrite Chainpur, with $\Delta^{17}O = +1.04‰$ (ref. 20). Furthermore, we have measured individual chondrules from both the carbonaceous chondrite Allende and the ordinary chondrite Chainpur for Fe isotopes. It has been documented[3] that chondrules from carbonaceous chondrites and ordinary chondrites are distinctively different in oxygen-isotope features, and it has been argued that these two sets of chondrules sampled the solar nebula in different regions or at different times[3]. So we expect that if any iron-isotope anomalies were inherited from circumstellar or interstellar mediums by the parent-body materials, they would probably have been revealed within this sample suite.

As a moderately volatile element, iron is depleted in refractory presolar grains such as corundum (Al_2O_3), and no attempt has been made so far to assess these phases for possible presolar iron-isotope signatures. We note, however, that isotopic anomalies of iron—as well as nickel and chromium, which have similar volatilities to iron—have been claimed to exist in some calcium- and aluminium-rich refractory inclusions (CAIs)[21–23]. Also, chromium-isotope anomalies have been found in leachates of some meteorites[24,25]. This demonstrates that iron isotopes were unlikely to have been initially homogeneous, and that their homogeneity recorded in the Solar System material results from subsequent processes taking place within the solar nebula.

This study shows that the solar nebula probably underwent events of isotope homogenization at an early stage, then subsequently fractionated in a mass-dependent manner for metal isotopes before (or during) the formation of chondrules and the parent bodies of meteorites. The homogeneity of iron isotopes in the early solar nebula is in marked contrast to the widespread oxygen-isotope anomalies recorded in meteorites[1–4]. But this apparent conflict could be reconciled if the latter anomalies resulted predominantly from chemical reactions that took place in the solar nebula, or if complete homogenization for oxygen isotopes had never been achieved between solid materials and the gaseous reservoir in the solar nebula. Because isotopic anomalies of Ti, Ca, Si, Cr and Fe have been reported in some CAIs[2,21–23,26–28], the isotope-homogenization events are unlikely to have pre-dated CAI formation, but must have preceded the formation of chondrules and the parent bodies of meteorites. □

Table 1 Fe-isotope data of terrestrial and extraterrestrial materials

Sample	Description	ϵ^{57}Fe	ϵ^{56}Fe
Carbonaceous Chondrites			
Allende (CV3)	Bulk sample (AG22)	–0.5	–0.4
Allende (CV3)	Matrix (AG23)	1.2	0.9
Allende (CV3)	Chondrule (AG38)	–8.8	–6.1
Allende (CV3)	Chondrule (A1)	–5.6	–3.9
Allende (CV3)	Chondrule (A2)	–7.2	–4.9
Allende (CV3)	Chondrule (A3)	3.9	2.5
Allende (CV3)	Chondrule (A6)	9.3	6.3
Murchison (CM2)	Bulk sample (BM5484)	–0.1	0.0
Orgueil (CI)	Bulk sample (BM3673)	6.0	3.8
Ordinary chondrites			
Chainpur (LL3)	Matrix (C19)	6.0	4.3
Chainpur (LL3)	Chondrule (C12)	–6.5	–4.6
Chainpur (LL3)	Chondrule (C14)	0.3	0.2
Chandakapur (L5)	Bulk sample (Mt4C)	–2.0	–1.5
Forest City (H5)	Metal fraction (Mt180)	–0.8	–0.6
Forest City (H5)	Duplicate	–0.6	–0.4
Enstatite chondrite			
Indarch (EH4)	Bulk sample	–1.1	–0.8
Achondrites			
Khor Temiki	Aubrite, bulk sample	0.1	0.0
Dyalpur	Ureilite, bulk sample	2.5	1.5
Stannern	Eucrite, bulk sample (Mt47)	–1.2	–0.6
Nakhla	Martian meteorite, bulk (Mt84)	–2.1	–1.4
Pallasites			
Krasnojarsk	Main group pallasite, metal fraction (Mt1)	–1.3	–0.9
Krasnojarsk	Duplicate	–1.5	–1.1
Imilac	Main group pallasite, metal fraction (Mt77)	–0.7	–0.5
Eagle Station	Non-main group pallasite, metal fraction	1.2	0.7
Iron meteorites			
Toluca (IAB)	Bulk sample (Mt70)	0.6	0.4
Cranbourne (IAB)	Bulk sample (Mt99)	2.0	1.5
Coahuila (IIAB)	Bulk sample (Mt83)	0.9	0.5
Carthage (IIIAB)	Bulk sample (Mt42)	0.6	0.4
Thunda (IIIAB)	Bulk sample (Mt46)	0.4	0.3
Bella Roca (IIIAB)	Bulk sample (Mt41)	0.6	0.2
Tazewell (IIICD)	Bulk sample (Mt33)	2.0	1.1
Terrestrial material			
Haematite	Specular; Cleator Moor, UK (OUM1927)	13.2	8.9
Haematite	Massive; Lake Superior (OUM858)	14.3	9.8
Haematite	Specular; Mt Vesuvius, Italy (OUM11387)	–5.4	–3.7
Magnetite	Rio La Marra Elba, Italy (OUM11421)	9.7	6.4
Magnetite	Kolar Peninsular, Russia (OUM29789)	2.1	1.5
Siderite	Newdorf, Harz Mt, Germany (OUM11479)	–6.8	–4.4

Measured $^{57}Fe/^{54}Fe$ and $^{56}Fe/^{54}Fe$ ratios are expressed as ϵ^{57}Fe and ϵ^{56}Fe which are deviations in parts per 10^4 from the Fe-isotope reference material IRMM-14 as following: $\epsilon^x Fe = [(R_{sample}/R_{standard} - 1)] \times 10,000$, where $R = {}^xFe/{}^{54}Fe$. Values of ϵ^{57}Fe and ϵ^{56}Fe for each sample are the averages of two or three separate analyses. Duplicate analyses include duplication of ion exchange chromatographic separation. The data quality was also controlled by repeated measurements of Romil Fe solution versus IRMM-14 Fe-isotope reference material during the run. The long-term repeatability for both ϵ^{57}Fe and ϵ^{56}Fe is 0.6ϵ at the 2-standard-deviation level, which gives an external precision of 0.6ϵ at the 2σ level. The internal precision for individual analysis is generally better than 0.3ϵ at the 2σ level. Symbols in brackets of the first column are meteorite types, and those in brackets of the second column are sample numbers.

Received 13 October 2000; accepted 15 May 2001.

1. Clayton, R. N., Grossman, L. & Mayeda, T. K. A component of primitive nuclear composition in carbonaceous meteorites. *Science* **182,** 485–488 (1973).
2. Clayton, R. N., Hinton, R. W. & Davis, A. M. Isotopic variations in the rock-forming elements in meteorites. *Phil. Trans. R. Soc. Lond. A* **325,** 483–501 (1988).
3. Clayton, R. N. Oxygen isotopes in meteorites. *Annu. Rev. Earth Planet. Sci.* **21,** 115–149 (1993).
4. Young, E. D. & Russell, S. S. Oxygen reservoirs in the early solar nebula inferred from an Allende CAI. *Science* **282,** 452–455 (1998).
5. Clayton, D. D. Isotope anomalies: Chemical memory of galactic evolution. *Astrophys. J.* **334,** 191–195 (1988).
6. Thiemens, M. H. & Heidenreich, J. E. The mass independent fractionation of oxygen: A novel isotope effect and its possible cosmochemical implications. *Science* **219,** 1073–1075 (1983).
7. Thiemens, M. H. Atmosphere science—Mass-independent isotope effects in planetary atmospheres and the early solar system. *Science* **283,** 341–345 (1999).
8. Cliff, S. S. & Thiemens, M. H. The $^{18}O/^{16}O$ and $^{17}O/^{16}O$ ratios in atmospheric nitrous oxide: A mass-independent anomaly. *Science* **278,** 1774–1776 (1997).
9. Rockmann, T. *et al.* Mass-independent oxygen isotope fractionation in atmospheric CO as a result of the reaction CO + OH. *Science* **281,** 544–546 (1998).
10. Bao, H. *et al.* Anomalous ^{17}O compositions in massive sulphate deposits on the Earth. *Nature* **406,** 176–178 (2000).
11. Bao, H., Campbell, D. A., Bockheim, J. G. & Thiemens, M. H. Origin of sulphate in Antarctic dry-valley soils as deduced from anomalous ^{17}O compositions. *Nature* **407,** 499–502 (2000).
12. Arnett, D. *Supernovae and Nucleosynthesis* (Princeton Univ. Press, Princeton, 1996).
13. Halliday, A. N. *et al.* Applications of multiple collector ICPMS to cosmochemistry, geochemistry and paleoceanography. *Geochim. Cosmochim. Acta* **62,** 919–940 (1998).
14. Zhu, X. K., O'Nions, R. K., Guo, Y., Belshaw, N. S. & Rickard, D. Determination of natural Cu-isotope variation by plasma-source mass spectrometry: implications for use as geochemical tracers. *Chem. Geol.* **163,** 139–149 (2000).

15. Zhu, X. K., O'Nions, R. K., Guo, Y. & Reynolds, B. C. Secular variation of iron isotopes in North Atlantic deep water. *Science* **287,** 2000–2002 (2000).
16. Belshaw, N. S., Zhu, X. K., Guo, Y. & O'Nions, R. K. High precision measurement of iron isotopes by plasma source mass spectrometry. *Int. J. Mass. Spectrom.* **197,** 191–195 (2000).
17. Marechal, C. N., Telouk, P. & Albarède, F. Precise analysis of copper and zinc isotopic compositions by plasma-source mass spectrometry. *Chem. Geol.* **156,** 251–273 (1999).
18. Clayton, R. N. & Mayeda, T. K. Formation of ureilites by nebular processes. *Geochim. Cosmochim. Acta* **52,** 1313–1318 (1988).
19. Clayton, R. N. & Mayeda, T. K. Oxygen isotope studies of achondrites. *Geochim. Cosmochim. Acta* **60,** 1999–2017 (1996).
20. Clayton, R. N. Mayeda, T. K., Goswami, J. N. & Olsen, E. J. Oxygen isotope studies of ordinary chondrites. *Geochim. Cosmochim. Acta* **55,** 2317–2337 (1991).
21. Volkening, J. & Papanastassiou, D. A. Iron isotope anomaly. *Astrophys. J.* **347,** L43–L46 (1989).
22. Volkening, J. & Papanastassiou, D. A. Zinc isotope anomaly. *Astrophys. J.* **358,** L29–L32 (1990).
23. Birck, J. L. & Lugmair, G. W. Nickel and chromium isotopes in Allende inclusions. *Earth Planet. Sci. Lett.* **90,** 131–143 (1988).
24. Rotaru, M., Birck, J. L. & Allègre, C. J. Clue to early solar system history from chromium isotopes in carbonaceous chondrites. *Nature* **358,** 465–470 (1992).
25. Podosek, F. A. *et al.* Thoroughly anomalous chromium in Orgueil. *Meteorit. Planet. Sci.* **32,** 617–627 (1997).
26. Niemeyer, S. & Lugmair, G. W. Titanium isotopic anomalies in meteorites. *Geochim. Cosmochim. Acta* **48,** 1401–1416 (1984).
27. Niemeyer, S. & Lugmair, G. W. Ubiquitous isotopic anomalies in Ti from normal Allende inclusions. *Earth Planet. Sci. Lett.* **53,** 211–225 (1981).
28. Papanastassiou, D. A. Chromium isotopic anomalies in the Allende meteorite. *Astrophys. J.* **308,** L27–L30 (1986).

Acknowledgements

We thank N. S. Belshaw for assistance with mass spectrometry; A. Galy for discussions and for providing solution aliquots of some samples analysed; G. Turner and F. Albarède for comments on the manuscript; and M. Price for providing samples of the Mt and OUM series. This work was supported by the Natural Environment Research Council.

Correspondence and requests for materials should be addressed to X.K.Z. (e-mail: xiangz@earth.ox.ac.uk).

Entanglement of the orbital angular momentum states of photons

Alois Mair*, Alipasha Vaziri, Gregor Weihs & Anton Zeilinger

Institut für Experimentalphysik, Universität Wien, Boltzmanngasse 5, 1090 Wien, Austria

Entangled quantum states are not separable, regardless of the spatial separation of their components. This is a manifestation of an aspect of quantum mechanics known as quantum non-locality[1,2]. An important consequence of this is that the measurement of the state of one particle in a two-particle entangled state defines the state of the second particle instantaneously, whereas neither particle possesses its own well-defined state before the measurement. Experimental realizations of entanglement have hitherto been restricted to two-state quantum systems[3–6], involving, for example, the two orthogonal polarization states of photons. Here we demonstrate entanglement involving the spatial modes of the electromagnetic field carrying orbital angular momentum. As these modes can be used to define an infinitely dimensional discrete Hilbert space, this approach provides a practical route to entanglement that involves many orthogonal quantum states, rather than just two Multi-dimensional entangled states could be of considerable importance in the field of quantum information[7,8], enabling, for example, more efficient use of communication channels in quantum cryptography[9–11].

Multi-dimensional entanglement is a way—in addition to multi-particle entanglement—to extend the usual two-dimensional two-particle state. There have been suggestions[12,13] (and only a proof-of-principle experiment[14]) as to how to realize higher-order entanglement via multiport beam splitters. Here we present an experiment in which we used the spatial modes of the electromagnetic field carrying orbital angular momentum to create multi-dimensional entanglement. The advantage of using these modes to create entanglement is that they can be used to define an infinitely dimensional discrete (because of the quantization of angular momentum) Hilbert space.

The experimental realization proceeded in the following two steps. First, we confirmed that spontaneous parametric down-conversion conserves the orbital angular momentum of photons. This was done for pump beams carrying orbital angular momenta of $-\hbar$, 0 and $+\hbar$ per photon, respectively. Second, we showed that the state of the down-converted photons can not be explained by assuming classical correlation—in the sense that the photon pairs produced are just a mixture of the combinations allowed by conservation of angular momentum. We proved that, in contrast, they are a coherent superposition of these combinations, and hence they have to be considered as entangled in their orbital angular momentum. After completion of the experimental work presented here, related theoretical work was brought to our attention[15,16].

We will now discuss in order the two steps mentioned above. For paraxial light beams, Laguerre–gaussian (LG) modes (Fig. 1) define a possible set of basis vectors. As predicted[17] and observed[18], LG modes carry an orbital angular momentum for linearly polarized light that is distinct from the intrinsic angular momentum of photons associated with their polarizations. This external angular momentum of the photon states is the reason why they have been suggested for gearing micromachines, and it has been shown that they can be used as optical tweezers[19–21].

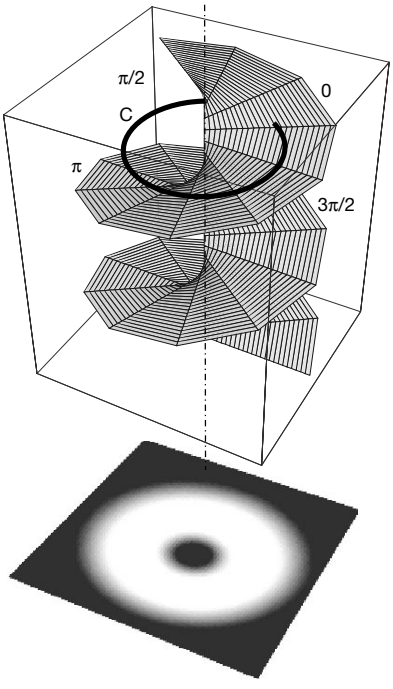

Figure 1 The wave front (top) and the intensity pattern (bottom) of the simplest Laguerre–gaussian (LG_p^l) or 'doughnut' mode. The index l is referred to as the winding number, and $(p + 1)$ is the number of radial nodes. Here we only consider cases of $p = 0$. The customary gaussian mode can be viewed as an LG mode with $l = 0$. The handedness of the helical wave fronts of the LG modes is linked to the sign of the index l, and can be chosen by convention. The azimuthal phase term $\exp il\phi$ of the LG modes results in helical wave fronts. The phase variation along a closed path C around the beam centre is $2\pi l$. Therefore, in order to fulfil the wave equation, the intensity has to vanish in the centre of the beam.

* Present address: Harvard-Smithsonian Center for Astrophysics, 60 Garden Street, Cambridge, Massachusetts 02138, USA.